Gas Marbles: Much Stronger than Liquid Marbles

yousra Timounay, Olivier Pitois, Florence Rouyer

▶ **To cite this version:**

yousra Timounay, Olivier Pitois, Florence Rouyer. Gas Marbles: Much Stronger than Liquid Marbles. Physical Review Letters, American Physical Society, 2017, 118 (22), 5 p. 10.1103/PhysRevLett.118.228001 . hal-01634940

HAL Id: hal-01634940

https://hal.archives-ouvertes.fr/hal-01634940

Submitted on 17 Apr 2018

HAL is a multi-disciplinary open access archive for the deposit and dissemination of scientific research documents, whether they are published or not. The documents may come from teaching and research institutions in France or abroad, or from public or private research centers.

L'archive ouverte pluridisciplinaire **HAL**, est destinée au dépôt et à la diffusion de documents scientifiques de niveau recherche, publiés ou non, émanant des établissements d'enseignement et de recherche français ou étrangers, des laboratoires publics ou privés.

Gas Marbles: Much Stronger than Liquid Marbles

Yousra Timounay,[1] Olivier Pitois,[1] and Florence Rouyer[2]
[1]Université Paris-Est, Laboratoire Navier, UMR 8205 CNRS, ENPC ParisTech, IFSTTAR, 2 allée Kepler, 77 420 Champs-Sur-Marne, France
[2]Université Paris-Est, Laboratoire Navier, UMR 8205 CNRS, ENPC ParisTech, IFSTTAR, 5 boulevard Descartes, 77 454 Champs-Sur-Marne, France
(Received 30 January 2017; published 2 June 2017)

Enwrapping liquid droplets with hydrophobic particles allows the manufacture of so-called "liquid marbles" [Aussillous and Quéré Nature (London) **411**, 924 (2001); Mahadevan **411**, 895 (2001)]. The recent intensive research devoted to liquid marbles is justified by their very unusual physical and chemical properties and by their potential for various applications, from microreactors to water storage, including water pollution sensors [Bormashenko Curr. Opin. Colloid Interface Sci. **16**, 266 (2011)]. Here we demonstrate that this concept can be successfully applied for encapsulating and protecting small gas pockets within an air environment. Similarly to their liquid counterparts, those new soft-matter objects, that we call "gas marbles," can sustain external forces. We show that gas marbles are surprisingly tenfold stronger than liquid marbles and, more importantly, they can sustain both positive and negative pressure differences. This magnified strength is shown to originate from the strong cohesive nature of the shell. Those interesting properties could be exploited for imprisoning valuable or polluted gases or for designing new aerated materials.

DOI: 10.1103/PhysRevLett.118.228001

During the past few decades, considerable research work has been devoted to particles attached to liquid-gas interfaces. Such particulate interfaces give rise to abundant and technologically important products, including foams and emulsions [1–6]. One of these products, known as "liquid marbles" [7,8], is a liquid drop coated with micro- or nanoscale hydrophobic particles, showing extreme mobility on solid substrates [7]. It has already been demonstrated that liquid marbles possess a potential for various applications [9] such as gas sensing [10], chemical microreactors [11], indicator of water pollution [12], and manipulation of small quantities of liquids (microfluidics) [13]. Recently, particle-covered bubbles in water have been produced as well [14]. Similarly to their liquid counterparts, the dissolution of those bubbles can be reduced or even stopped, and their shape can be nonspherical [15], revealing the mechanical stability of the protecting shell. Dedicated experiments have probed the corresponding mechanical strength: It has been shown that armored drops or bubbles of diameter D_b can oppose liquid and gas removal up to applied pressures equal to $4\gamma/D_b$, i.e., the Laplace pressure of the particle-free drop or bubble with γ being the surface tension of the liquid-gas interface [14,16–18]. For larger particle-to-drop or bubble size ratio, i.e., $D_P/D_b \geq 0.1$, faceted morphologies and granular arches occur, and the magnitude of the collapse pressure increases up to twice the Laplace pressure [14,16].

The system we study is a gas volume of the order of a few hundreds of mm^3 delimited from the outer air by a liquid film entrapping a compact monolayer of particles as shown in Fig. 1. This new object distinguishes from the so-called liquid marble by the fact that the delimiting armor counts two liquid-gas interfaces, instead of a single one, and the inner phase is gas, instead of liquid. We propose to call it a "gas marble." As shown in the following, the

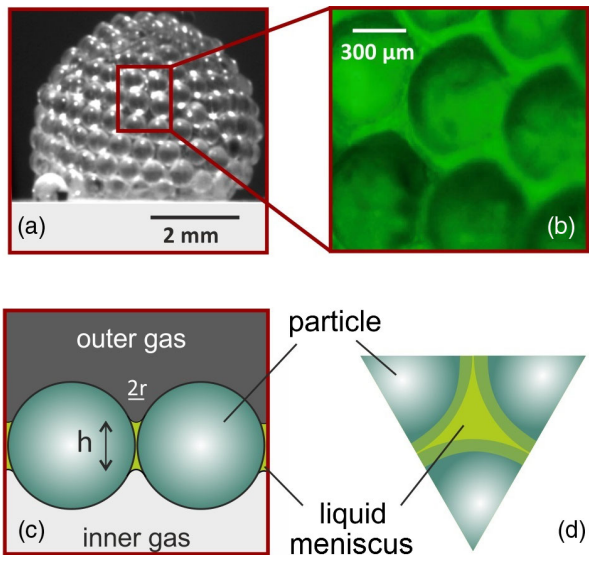

FIG. 1. The so-called gas marble elaborated and studied in this work. (a) Image of a gas marble ($D_p = 590\ \mu$m and $D_b = 5$ mm). (b) Enlargement of the particle layer (fluorescent liquid): The liquid phase can be distinguished by the curved liquid-gas interface around each particle contact. (c) Sketch of the cross section revealing the structure of the cohesive granular shell. (d) Sketch of a meniscus connecting three particles.

 © 2017 American Physical Society

presence of the two interfaces on the shell provides exceptional stability properties to the gas marble. Indeed, gas marbles can resist both gas removal and gas loading, up to applied pressures equal to 10 times the Laplace pressure. This remarkable stability is attributed to capillary-induced cohesion arising from the geometrical configuration of the confining liquid film between the particles forming the shell.

Gas marbles we elaborate consist of air volumes delimited by a liquid film, of thickness h, supporting a compact monolayer of particles (Fig. 1). They are spherical when formed, but, like liquid marbles, the contacting part with the support flattens. The liquid phase we use is a surfactant (SDS) solution at a concentration close to the critical micellar concentration, allowing the formation of stable thin liquid films. The surface tension γ is equal to 36 mN/m. Particles, for their part, are monodisperse polystyrene beads with a diameter $D_P \sim 100$ μm. They are thus larger than the liquid film thickness, i.e., $h < D_P$. Gas marbles are formed through a process inspired from the generation of classical soap bubbles: dipping and removing a solid horizontal frame from a soap solution. Here the main difference comes from the fact that the solution interface supports a particle raft, so, during this process, a particulate film can be created [19]. For the large frames and particles we used, resorting to blowing for forming the bubbles was not necessary; the particulate film detaches from the frame due to gravity and closes over itself to form a bubble. More details concerning the generation of gas marbles can be found in Supplemental Material (text and movie) [20].

To characterize the properties of gas marbles, we performed experiments consisting in studying their behavior when they undergo inner pressure variations. We studied their behavior during inflation and deflation by connecting them to a syringe and to a pressure sensor (Freescale, range from 0 to 10 kPa and sensitivity equal to 10 Pa). The inner pressure P_b is measured by the pressure sensor, and, thanks to a syringe pump, the volume of the syringe is controlled. Increasing the syringe volume results in a decrease of the gas marble inner pressure P_b, and vice versa. Volume variations are performed at a constant flow rate equal to 0.06 ml/min during all of our experiments. Two cameras placed above and on the side allow us to follow the evolution of the shape of gas marbles.

Figure 2 shows an example of top and side views of a gas marble during an inflation experiment, as well as an example of the evolution of the inner pressure relative to atmospheric pressure $P_b - P_{\text{atm}}$, as a function of the variation of the syringe volume ΔV. The same qualitative behavior has been observed during all inflation experiments. At $t = 0$, the relative inner pressure is zero: $P_{b0} = P_{\text{atm}}$. This result strongly differs from that of conventional armored drops and bubbles [14,16–18] and soap bubbles for which Laplace's law applies, i.e., $\Delta P_{\text{cap}} = 8\gamma/D_b$. This behavior can be explained by

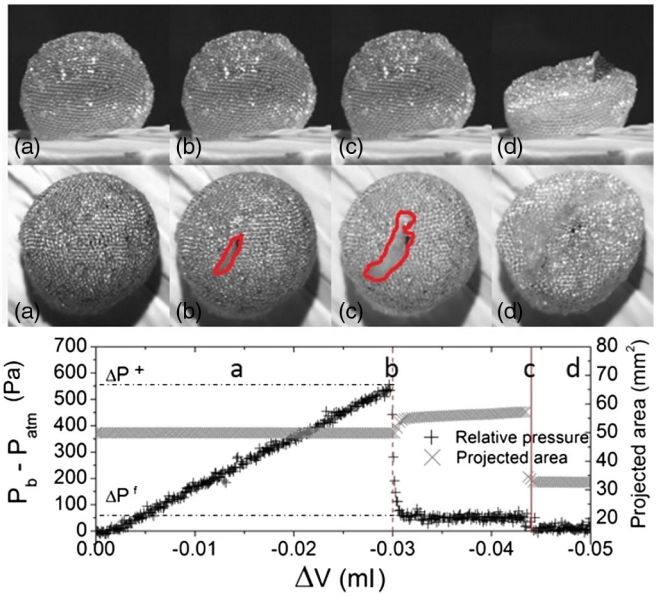

FIG. 2. Side and top views of a gas marble ($D_p = 315$ μm and $D_b = 6$ mm) during an inflation experiment for successive volume variations ΔV of the gas reservoir. The relative inner pressure and side projected area are plotted versus ΔV. (a) The inner pressure increases linearly with ΔV, while the armor is static up to a critical pressure difference ΔP^+. (b) A liquid fracture arises, and it is accompanied by a sudden increase of the side-view projected area, as well as a steep pressure drop from a maximum value, noted ΔP^+, down to a plateau value, noted $\Delta P^f \sim \Delta P^+/10$. While the fracture (contour is highlighted in red) area keeps growing (b),(c), the projected area and inner pressure remain constant until the liquid film on top of the bubble ends up bursting, resulting in the release of internal pressure.

compressive stress developing in the compact particle monolayer and balancing surface tension forces [14,16]. During inflation experiments, gas marbles go through a first regime, denoted "a" in Fig. 2, where they keep their initial shape. During this regime, $P_b - P_{\text{atm}}$ increases linearly from a zero value. In considering the gas volume V_0 composed of the particulate bubble, the syringe, and the connecting pipes, then, thanks to the ideal gas law, one can write $P_b - P_{\text{atm}} = P_b - P_{b0} = P_{\text{atm}}[V_0/(V_0 + \Delta V) - 1]$. As $|\Delta V|/V_0 \ll 1$ ($V_0 \sim 5$ ml and $|\Delta V| \sim 0.05$ ml), the expected pressure evolution during the first regime is $P_b - P_{\text{atm}} \simeq -P_{\text{atm}}\Delta V/V_0$. Proportionality coefficient P_{atm}/V_0 is equal to $\sim 2 \times 10^4$ Pa/ml, which is in quantitative agreement with the experimental slope in Fig. 2 equal to 1.8×10^4 Pa/ml. The first regime a ends when a unique fracture appears at the top of gas marbles. This event is accompanied by a sudden increase of the gas marble projected area and a steep pressure drop ("b" in Fig. 2) from a maximum relative pressure, noted ΔP^+, down to a plateau value noted $\Delta P^f \sim \Delta P^+/10$. Once the fracture appears, its area keeps on growing until the liquid film on top of the bubble ends up bursting. During this stage (between b and c in Fig. 2), the relative inner pressure of

particulate bubbles ΔP^f is equal to the Laplace pressure for soap bubbles (see Supplemental Material [20]). This result shows that the gas marble behavior is due to the synergetic actions of both the liquid interfaces and the contacting particles.

Thanks to inflation experiments, we measured the maximal inner overpressure ΔP^+ that the gas marble shell can resist.

In addition, we performed deflation experiments by increasing the volume of the syringe connected to gas marbles. Figure 3 shows an example of successive images taken during the deflation process. All gas marbles go through a first regime, noted a, where no deformation is observed despite the increase of the syringe's volume. Similarly to the inflation experiment, the pressure is measured to decrease linearly. After this regular regime, the inner relative pressure tends to increase punctually in response to small amplitude deformations of the gas marbles. These very small deformations can be revealed by the steep evolutions of the projected surface area correlated to each pressure peak. The number of pressure peaks per experiment has varied from one experiment to another between 0 and 4. After these small perturbations that do not seem to jeopardize the bubble stability, the pressure keeps on decreasing until the gas marbles end up collapsing at ΔP^- (d in Fig. 3). The relative inner pressure returns back steeply to zero value after the collapse, probably because the shell is pierced due to the ejection of one or more particles. After the collapse, the gas marbles keep on flattening under their own weight (e in Fig. 3). ΔP^- is thus the critical stability threshold of gas marbles when deflated. Imposing a larger underpressure results in the collapse of the gas marble.

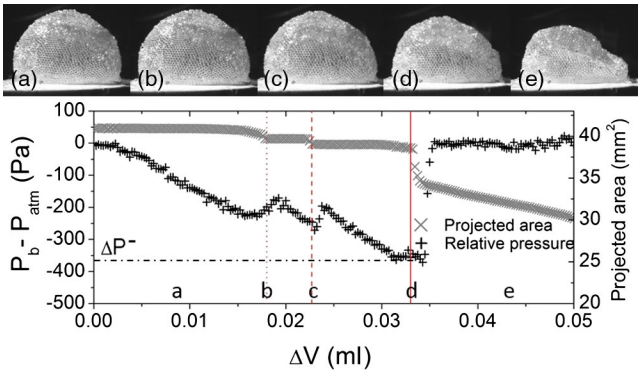

FIG. 3. Side views of a gas marble ($D_p = 250\ \mu$m, $D_b = 10$ mm) during the deflation experiment for successive volume variations ΔV of the gas reservoir. The relative inner pressure and side projected area are plotted versus ΔV. (a)–(d) The inner pressure decreases quasilinearly with ΔV down to a critical pressure difference ΔP^-. Few pressure jumps can be observed, and they are found to be associated to small peaks of the projected area (b),(c). At the critical inner underpressure value ΔP^-, the bubble collapses (d). Then the inner pressure value returns back steeply to atmospheric pressure, while the bubble shrinks (e).

The critical relative pressure values ΔP^+ and ΔP^-, measured within both inflation and deflation conditions, respectively, are plotted in Fig. 4 as a function of bubble diameters D_b, for several particle diameters D_p. Note that those pressure values have been reduced by Laplace pressure ΔP_{cap} of the corresponding particle-free bubbles. Remarkably, these critical pressures vary significantly neither with particle diameters nor with bubble diameters nor with D_p/D_b, in the range of sizes explored in this study (see Supplemental Material [20]).

Contrary to classical armored bubbles and drops, gas marbles can sustain both negative and positive applied relative pressures from their initial state. The measured values for the critical pressure, that gas marbles can sustain within inflation or deflation processes, are approximatively the same in absolute value. For negative pressures, with respect to liquid marbles [16–18], the stability range is increased by a factor of 10, revealing therefore exceptional properties for resisting against collapse. But, obviously, the

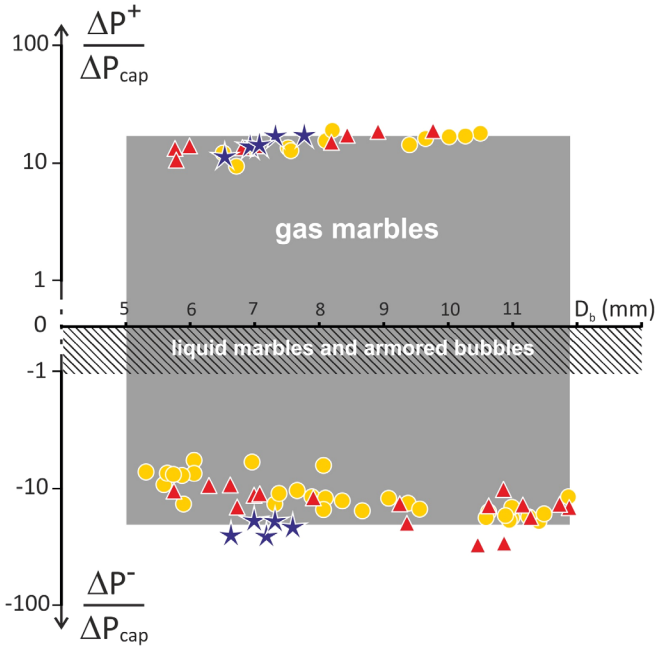

FIG. 4. Normalized critical overpressures ($\Delta P^+/\Delta P_{cap}$) and underpressures ($\Delta P^-/\Delta P_{cap}$) measured for gas marbles within both inflation and deflation conditions, respectively, as a function of bubble diameter D_b, for several particle diameters D_p (250 μm, open circle; 315 μm, star; 590 μm, triangle). Laplace pressure $\Delta P_{cap} = 8\gamma/D_b$ is the pressure at equilibrium of the corresponding particle-free bubbles. The stability range of gas marbles is colored in gray, and it is compared to the stability range for liquid marbles and armored bubbles (dashed area [17,18]) for which the Laplace pressure $\Delta P_{cap} = 4\gamma/D_b$ corresponds to the particle-free drop or bubbles with one liquid interface.

drastic difference to liquid marbles comes from the capacity of gas marbles to resist against fluid loading up to 10 times the Laplace pressure of the corresponding bare bubble, whereas liquid marbles do not possess any strength for such a solicitation mode. In the next paragraphs, we bring physical elements for understanding the exceptional stability of gas marbles.

The origin of this remarkable strength is expected to be related to particle confinement imposed by the double interface delimiting the bubble, whereas a single interface is present for armored bubbles and drops. The observation of the shell reveals that the liquid distributes within the pore space of the particle monolayer and forms a thick capillary structure. This geometrical configuration is reminiscent of the so-called "capillary state" of wet granular agglomerates [21], which is known as a cohesive material.

Let us now consider the behavior of gas marbles in assuming that their protecting shell is a cohesive granular monolayer of thickness h. The equilibrium of a thin spherical shell, i.e., $h/D_b \ll 1$, implies that [22] $P_b - P_{\mathrm{atm}} \approx 4h\sigma_{\mathrm{sh}}/D_b$, where, for the present situation, $\sigma_{\mathrm{sh}} = \sigma_{\mathrm{cap}} + \sigma_p$ is the circumferential stress (Hoop stress) arising in the shell from both capillarity (σ_{cap}) and particle contact (σ_p) effects. The initial pressure of gas marbles has been measured to be $P_b \approx P_{\mathrm{atm}}$, whereas for classical bubbles $P_b = P_{\mathrm{atm}} + \Delta P_{\mathrm{cap}}$, which corresponds to $\sigma_p = 0$ and $\sigma_{\mathrm{cap}} = 2\gamma/h$, would be observed. This result can be explained by the prestressing of the particle monolayer, i.e., $\sigma_p < 0$, due to cohesive (attractive) forces induced by the confining interfaces, i.e., $\sigma_{\mathrm{cap}} > 2\gamma/h$. Therefore, the initial configuration of gas marbles is described by $\sigma_{\mathrm{cap}} + \sigma_p = 0$. As P_b increases, the magnitude of σ_p is expected to decrease, because part of the capillary stress is supported by the bubble internal pressure. Just before the rupture of the shell at $P_b - P_{\mathrm{atm}} = \Delta P^+ \approx 10\Delta P_{\mathrm{cap}}$, the particles barely touch one another, and, thus, $\sigma_p = 0$ and $\sigma^+_{\mathrm{cap}} \approx D_b \Delta P^+/4h \approx 2(\gamma/h)(\Delta P^+/\Delta P_{\mathrm{cap}}) \approx 20\gamma/h$. The capillary stress should be related to the mean radius of curvature describing the liquid-gas interface within the monolayer pore space: $\sigma^+_{\mathrm{cap}} \approx \gamma/r$, which means that $r/h \approx 1/20$. Moreover, from the geometrical configuration of the capillary interface around contacts between spherical particles, it comes that $r/h \approx h/4D_p$, which is reconcilable with lengths estimated from Fig. 1 and implies $\Delta P^+/\Delta P_{\mathrm{cap}} \approx 2D_p/h$. As we do not measure any significant dependence of ΔP^+ with D_p, it appears, therefore, that $h \propto D_p$, which suggests that the volume of liquid carried out by particles during the production process is rather set by the particle size. Moreover, the slight increase of $\Delta P^+/\Delta P_{\mathrm{cap}}$ with D_b we observe in Fig. 4 can be interpreted as a decrease of h when D_b increases. A dedicated study of the production process would allow clarifying this issue. Note that the particles have to be packed for the capillary cohesion to exist. Therefore, as soon as the monolayer fractures, a thin particle-free soap film appears, and the capillary stress drops down to the classical value, i.e., $\sigma^f_{\mathrm{cap}} = 2\gamma/h$, and the Laplace pressure is consequently recovered: $\Delta P^f = \Delta P_{\mathrm{cap}} = 8\gamma/D_b$ (see Supplemental Material [20]).

As the resistance against collapse is probed, the decrease of the internal pressure is balanced by the compressive stress due to particle contacts in the monolayer, i.e., $\sigma_p < 0$, as observed for classical armored bubbles and drops [14,16,18]. However, the cohesive nature of the shell allows for the collapse pressure to drastically increase with respect to reported collapse pressure values. As the onset of collapse is induced by particle displacements out of the monolayer plane [14,16], the basic argument to explain our result is that here those particle displacements are strongly restrained by capillary forces acting between particles as springs that are stiffer than those corresponding to classical armored systems. In order to get deeper into that issue, and to compare the collapse strengths, it is convenient to introduce the so-called "effective surface tension" of gas marbles, measured at the onset of fracture opening: $\gamma_{\mathrm{eff}} = h\sigma^+_{\mathrm{cap}} \approx 20\gamma$. Therefore, the ratio $|\Delta P^-|/\gamma_{\mathrm{eff}} \approx 10\Delta P_{\mathrm{cap}}/\gamma_{\mathrm{eff}} \approx 4/D_b$. Note that, for classical armored bubbles and drops (single interface), this ratio is also equal to $\Delta P_{\mathrm{cap}}/\gamma = 4/D_b$. Consequently, the collapse mechanisms seem to be the same, except that the restoring capillary forces are 10 times larger for gas marbles. The existence of such a high pressure threshold, that needs to be exceeded before gas marbles deform within deflation conditions, is analogous to the behavior of solid elastic shells, whose collapse pressure is $(16E \cdot D_P^2/D_b^2)$ [22], where E is the bulk elastic modulus of the shell. From ΔP^- we estimate the expected value for this modulus: $E \approx 20$ kPa. This value is at least 100 times larger than the values reported for particles rafts [23,24] and classical armored drops [16]. This highlights again how the strength of gas marbles differs from the strength of classical armored bubbles and drops.

Particulate bubbles we generate can sustain negative and positive relative pressures of amplitude ~10 times greater than the Laplace pressure. The strong capillary cohesion arising in the shell is at the origin of the reported magnified strength of those gas marbles. In terms of applications, the highly resistive bubbles we present in this work can be beneficial for the stabilization of foams and emulsions, by inhibiting coarsening and, therefore, promoting the elaboration of well-controlled light materials. In the context of remediation, new gas encapsulation processes could be developed by the use of such resistive bubbles. For example, gas marbles containing up to 0.5% of insoluble gas in the liquid shell are expected to be stable without significant gas exchange with their environment.

All the authors thank Even Ou for conducting some experiments and are grateful to Elise Lorenceau for

discussions and comments on the manuscript. We gratefully acknowledge financial support from French Space Agency (convention CNES/70980) as well as funding from IFSTTAR.

[1] S. U. Pickering, J. Chem. Soc. Dalton Trans. **91**, 2001 (1907).
[2] B. P. Binks and T. S. Horozov, Angew. Chem. **117**, 3788 (2005).
[3] B. P. Binks and R. Murakami, Nat. Mater. **5**, 865 (2006).
[4] U. T. Gonzenbach, A. R. Studart, E. Tervoort, and L. J. Gauckler, Langmuir **22**, 10983 (2006).
[5] A. Stocco, W. Drenckhan, E. Rio, D. Langevin, and B. P. Binks, Soft Matter **5**, 2215 (2009).
[6] E. Dickinson, Curr. Opin. Colloid Interface Sci. **15**, 40 (2010).
[7] P. Aussillous and D. Quéré, Nature (London) **411**, 924 (2001).
[8] L. Mahadevan, Nature (London) **411**, 895 (2001).
[9] E. Bormashenko, Langmuir **33**, 663 (2017).
[10] J. Tian, T. Arbatan, X. Li, and W. Shen, Chem. Commun. (Cambridge) **46**, 4734 (2010).
[11] P. S. Bhosale and M. V. Panchagnula, Langmuir **26**, 10745 (2010).
[12] E. Bormashenko and A. Musin, Appl. Surf. Sci. **255**, 6429 (2009).
[13] Y. Zhao, J. Fang, H. Wang, X. Wang, and T. Lin, Adv. Mater. **22**, 707 (2010).
[14] M. Abkarian, A. B. Subramaniam, S.-H. Kim, R. J. Larsen, S.-M. Yang, and H. A. Stone, Phys. Rev. Lett. **99**, 188301 (2007).
[15] A. B. Subramaniam, M. Abkarian, L. Mahadevan, and H. A. Stone, Nature (London) **438**, 930 (2005).
[16] O. Pitois, M. Buisson, and X. Chateau, Eur. Phys. J. E **38**, 48 (2015).
[17] N. Taccoen, F. Lequeux, D. Z. Gunes, and C. N. Baroud, Phys. Rev. X **6**, 011010 (2016).
[18] C. Monteux, J. Kirkwood, H. Xu, E. Jung, and G. G. Fuller, Phys. Chem. Chem. Phys. **9**, 6344 (2007).
[19] Y. Timounay and F. Rouyer, Soft Matter **13**, 3449 (2017).
[20] See Supplemental Material at http://link.aps.org/supplemental/10.1103/PhysRevLett.118.228001for Gas Marbles: Much Stronger than Liquid Marbles - Supplemental material consisting of a movie showing a gas marble creation and a text giving details on the experimental method as well as plots and comments on the evolution of the pressure ΔPf during fracture and the effect of particle-to-bubble size ratios on the critical relative pressure values.
[21] D. Newitt and J. Conway-Jones, Trans. Inst. Chem. Eng. **422**, 36 (1958).
[22] L. D. Landau and E. Lifshitz, Cour. Theor. Phys. **109**, 3 (1986).
[23] D. Vella, P. Aussillous, and L. Mahadevan, Europhys. Lett. **68**, 212 (2004).
[24] C. Planchette, E. Lorenceau, and A.-L. Biance, Soft Matter **8**, 2444 (2012).
[25] E. Bormashenko, Curr. Opin. Colloid Interface Sci. **16**, 266 (2011).